

Exciton diffusion in two-dimensional metal-halide perovskites

Michael Seitz^{1,2}, Alvaro J. Magdaleno^{1,2}, Nerea Alcázar-Cano^{1,3}, Marc Meléndez^{1,3},

Tim J. Lubbers^{1,2}, Sanne W. Walraven^{1,2}, Sahar Pakdel⁴, Elsa Prada^{1,2},

Rafael Delgado-Buscalioni^{1,3}, and Ferry Prins^{1,2}

1. Condensed Matter Physics Center (IFIMAC), Autonomous University of Madrid, 28049 Madrid, Spain

2. Department of Condensed Matter Physics, Autonomous University of Madrid, 28049 Madrid, Spain

3. Department of Theoretical Condensed Matter Physics, Autonomous University of Madrid, 28049 Madrid, Spain

4. Department of Physics and Astronomy, Aarhus University, 8000 Aarhus C, Denmark

To whom correspondence should be addressed: ferry.prins@uam.es

Abstract

Two-dimensional perovskites, in which inorganic layers are stabilized by organic spacer molecules, are attracting increasing attention as a more robust analogue to the conventional three-dimensional metal-halide perovskites. However, reducing the perovskite dimensionality alters their optoelectronic properties dramatically, yielding excited states that are dominated by bound electron-hole pairs known as excitons, rather than by free charge carriers common to their bulk counterparts. Despite the growing interest in two-dimensional perovskites for both light harvesting and light emitting applications, the full impact of the excitonic nature on their optoelectronic properties remains unclear, particularly regarding the spatial dynamics of the excitons within the two-dimensional (2D) plane. Here, we present direct measurements of in-plane exciton transport in single-crystalline layered perovskites. Using time-resolved fluorescence microscopy, we show that excitons undergo an initial fast, intrinsic normal diffusion through the crystalline plane, followed by a transition to a slower subdiffusive regime as excitons get trapped. Interestingly, the early intrinsic exciton diffusivity depends sensitively on the choice of organic spacer. We find a clear correlation between the stiffness of the lattice and the diffusivity, suggesting exciton-phonon interactions to be dominant in determining the spatial dynamics of the excitons in these materials. Our findings provide a clear design strategy to optimize exciton transport in these systems.

Introduction

Metal-halide perovskites are a versatile material platform for light harvesting¹⁻⁵ and light emitting applications,^{6,7} combining the advantages of solution processability with high ambipolar charge carrier mobilities,^{8,9} high defect tolerance,¹⁰⁻¹² and tunable optical properties.¹³⁻¹⁵ Currently, the main challenge in the applicability of perovskites is their poor environmental stability.¹⁶⁻¹⁹ Reducing the dimensionality of the perovskite has proven to be one of the most promising strategies to yield a more stable performance.²⁰⁻²³ Perovskite solar cells with mixed 2D and 3D phases, for example, have been fabricated with >22% efficiencies²⁴ and stable performance for more than 10.000 hours,²⁵ while phase pure 2D perovskite solar cells have been reported with efficiencies above 18%.^{26,27} Likewise, significant stability improvements have been reported for phase pure 2D perovskites as the light emitting layer in LED technologies.²⁸⁻³⁴ The improved environmental stability in 2D perovskite phases is attributed to a better moisture resistance due to the hydrophobic organic spacers that passivate the inorganic perovskite sheets, as well as an increased formation energy of the material.²⁰⁻²³

However, the reduced dimensionality of 2D perovskites dramatically affects the charge carrier dynamics in the material, requiring careful consideration in their application in optoelectronic devices.³⁵⁻³⁷ 2D perovskites are composed of inorganic metal-halide layers, which are separated by long organic spacer molecules. They are described by their general chemical formula $L_2[ABX_3]_{n-1}BX_4$, where A is a small cation (e.g. methylammonium, formamidinium), B is a divalent metal cation (e.g. lead, tin), X is a halide anion (chloride, bromide, iodide), L is a long organic spacer molecule, and n is the number of octahedra that make up the thickness of the inorganic layer. The separation into few-atom thick inorganic layers yields strong quantum and dielectric confinement effects.³⁸ As a result, the exciton binding energies in 2D perovskites can be as high as several hundreds of meVs, which is around an order of magnitude larger than those found in bulk perovskites.³⁹⁻⁴¹ The excitonic character of the excited state is accompanied by an effective widening of the bandgap, an increase in the oscillator strength, and a narrowing of the emission spectrum.⁴⁰⁻⁴² The strongest confinement effects are observed for $n = 1$, where the excited state is confined to a single B-X-octahedral layer (see Figure 1a).

Light harvesting using 2D perovskites relies on the efficient transport of excitons and their subsequent separation into free charges.⁴³ This stands in contrast to bulk perovskites in which free charges are generated instantaneously thanks to the small exciton binding energy.³⁹ Particularly, with excitons being neutral quasi-particles, the charge extraction becomes significantly more challenging as they cannot be guided to the electrodes through an external electric field.⁴⁴ Excitons need to diffuse to an interface before the electron and hole can be efficiently separated into free charges.⁴⁵ On the other hand, for light emitting applications the spatial displacement is preferably inhibited, as a larger diffusion path increases the risk of encountering quenching sites which would reduce brightness. While charge transport in bulk perovskites has been studied in great detail, the mechanisms that dictate exciton transport in 2D perovskites remain elusive.⁴⁵ Moreover, it is unclear to what extent exciton transport can be controlled through variations in the perovskite composition.

Here, we report the direct visualization of exciton diffusion in 2D single-crystalline perovskites using time-resolved microscopy.⁴⁶ This technique allows us to follow the temporal evolution of a near-diffraction-limited exciton population with sub-nanosecond resolution and reveals the spatial and temporal exciton dynamics. We observe two different diffusion regimes. For early times, excitons follow normal diffusion, while for later times a subdiffusive regime emerges, which is attributed to the presence of trap states. Using the versatility of perovskite materials, we study the influence of the organic spacer on the diffusion dynamics of excitons in 2D perovskites. We find that between commonly used organic spacers (phenethylammonium, PEA, and butylammonium, BA), diffusivities and diffusion lengths can differ by one order of magnitude. We show that these changes are closely correlated with variations in the softness of the lattice, suggesting a dominant role for exciton-phonon coupling and exciton-polaron formation in the spatial dynamics of excitons in these materials. These insights provide a clear design strategy to further improve the performance of 2D perovskite solar cells and light emitting devices.

Results

We prepare single crystals of $n = 1$ phenethylammonium lead iodide $(\text{PEA})_2\text{PbI}_4$ 2D perovskite by drop-casting a saturated precursor solution onto a glass substrate,^{47–49} as confirmed by XRD analysis and photoluminescence spectroscopy (see methods section for details). Using mechanical exfoliation, we isolate single-crystalline flakes of the perovskite and transfer these to microscopy slides. The single-crystalline flakes have typical lateral sizes of tens to hundreds of micrometers and are optically thick. The use of thick flakes provides a form of self-passivation that prevents the typical fast degradation of the perovskite in ambient conditions.

To measure the temporal and spatial exciton dynamics, we create a near-diffraction-limited exciton population using a pulsed laser diode ($\lambda_{\text{ex}} = 405 \text{ nm}$) and an oil immersion objective (N.A. = 1.3). The image of the fluorescence emission of the exciton population is projected outside the microscope with high magnification (330x), as illustrated in Figure 1b. By placing a scanning avalanche photodiode (20 μm in size) in the image plane, we resolve the time-dependent broadening of the population with high temporal and spatial resolution. Figure 1c shows the resulting map of the evolution in space and time of the fluorescence emission intensity of an exciton population in $(\text{PEA})_2\text{PbI}_4$. The fluorescence emission intensity $I(x,t)$ is normalized at each point in time to highlight the broadening of the emission spot over time. Each time-slice $I(x,t_c)$ is well described by a Voigt function,⁵⁰ from which we can extract the variance $\sigma(t)^2$ of the exciton distribution at each point in time (Figure 1d). On a timescale of several nanoseconds, the exciton distribution broadens from an initial $\sigma(t = 0) = 171 \text{ nm}$ to $\sigma(t = 10 \text{ ns}) = 448 \text{ nm}$, indicating fast exciton diffusion.

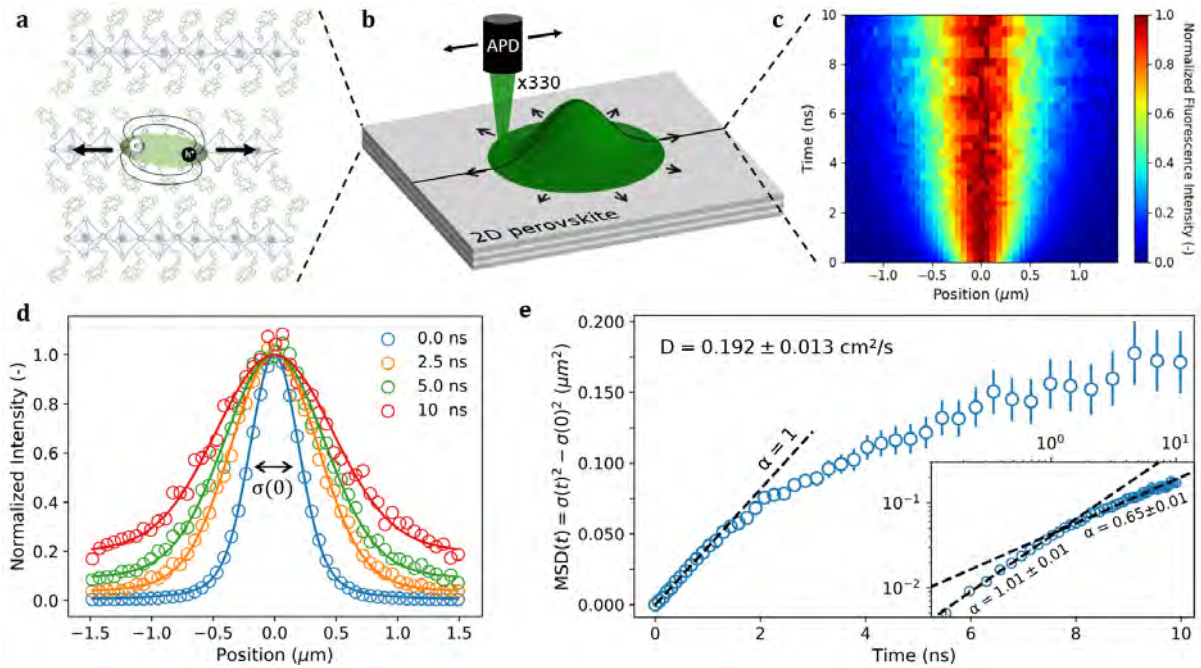


Figure 1. (a) Illustration of the (PEA)₂PbI₄ crystal structure, showing the perovskite octahedra sandwiched between the organic spacer molecules. (b) Schematic of the experimental setup. A near-diffraction limited exciton population is generated with a pulsed laser diode. The spatial and temporal evolution of the exciton population is recorded by scanning an avalanche photodiode through the magnified image of the fluorescence $I(x,t)$. (c) Fluorescence emission intensity $I(x,t)$ normalized at each point in time to highlight the spreading of the excitons. (d) Cross section of $I(x,t)$ for different times t_c . (e) Mean-square-displacement of the exciton population over time. Two distinct regimes are present: First, normal diffusion with $\alpha = 1$ is observed, which is followed by a subdiffusive regime with $\alpha < 1$. The inset shows a log-log plot of the same data, highlighting the two distinct regimes. Reported errors represent the uncertainty in the fitting procedure for $\sigma(t)^2$.

To analyze the time-dependent broadening of the emission spot in more detail, we study the temporal evolution of the mean-square-displacement (MSD) of the exciton population, given by $MSD(t) = \sigma(t)^2 - \sigma(0)^2$. Taking the one-dimensional diffusion equation as a simple approximation, it follows that $MSD(t) = 2Dt^\alpha$, which allows us to extract the diffusivity D and the diffusion exponent α from our measurement (see SI for derivation).^{46,50} In Figure 1e we plot the MSD as a function of time. Two distinct regimes can be observed: For early times ($t \lesssim 1$ ns) a fast linear broadening occurs with $\alpha = 1.01 \pm 0.01$, indicative of normal diffusion, while for later times ($t \gtrsim 1$ ns) the broadening becomes progressively slower with $\alpha = 0.65 \pm 0.01$, suggesting a regime of trap-state limited exciton transport (see SI for more details). The two regimes are clearly visible in the inset of Figure 1e, where different slopes correspond to different α values. From these measurements, a diffusivity of 0.192 ± 0.013 cm²/s is found for (PEA)₂PbI₄.

The role of trap-states in perovskite materials is well studied and is generally attributed to the presence of imperfections at the surface of the inorganic layer.⁵¹ These lower-energy sites lead to a subdiffusive behavior as a subpopulation of excitons becomes trapped. To test the influence of trap states, we have performed diffusion measurements in the presence of a continuous wave (CW) background excitation of varying intensity (Figure 2). The background excitation leads to a steady state population of excitons, which fill some of the traps and thereby reduce the effective trap density. To minimize the invasiveness of the measurement itself, the repetition rate and fluence were reduced to a minimum (see SI for details). In the absence of any background illumination, we find a strongly subdiffusive diffusion exponent of $\alpha = 0.48 \pm 0.02$. As the background intensity is increased, an increasing α is observed, indicative of trap state filling. Ultimately, a complete elimination of subdiffusion ($\alpha = 0.99 \pm 0.02$) is obtained at a background illumination power of 60 mW/cm². For comparison, this value corresponds roughly to a 2.5 Sun illumination. Additionally, we observe that the onset of the subdiffusive regime is delayed as more and more trap states are filled, as represented by the increasing t_{split} parameter (see Figure 2b, bottom panel).

To gain theoretical insights and quantitative predictions concerning the observed subdiffusive behavior of excitons and its relation with trap state densities, we performed numerical simulations based on Brownian dynamics of individual excitons diffusing in a homogeneously distributed and random trap field (see SI for details). In addition, we developed a coarse-grained theoretical model based on continuum diffusion of the exciton concentration (see SI for details). The continuum theory predicts an exponential decay of the exciton diffusion coefficient,

$$\frac{1}{2} \frac{dMSD(t)}{dt} = D(t) = D \exp\left(-\frac{D}{\lambda^2} t\right) \quad (1)$$

where λ is the average distance between traps. The integral of this expression leads to

$$MSD(t) = 2\lambda^2 \left[1 - \exp\left(-\frac{D}{\lambda^2} t\right)\right], \quad (2)$$

which, as shown in Figure 2c, successfully reproduces both experimental and numerical results and allows us to accurately determine the value of the intrinsic trap state density, yielding $1/\lambda^2 = 22 \mu\text{m}^{-2}$. The inset in Figure 2c shows the evolution of the effective trap state density $1/\lambda^2$ with increasing illumination intensity. We note that the exponential decay of equation (1) allows for a more intuitive characterization of $D(t)$ by relating the subdiffusion directly to the trap density $1/\lambda^2$ rather than relying on the subdiffusive exponent α of a power law commonly used in literature.⁴⁶

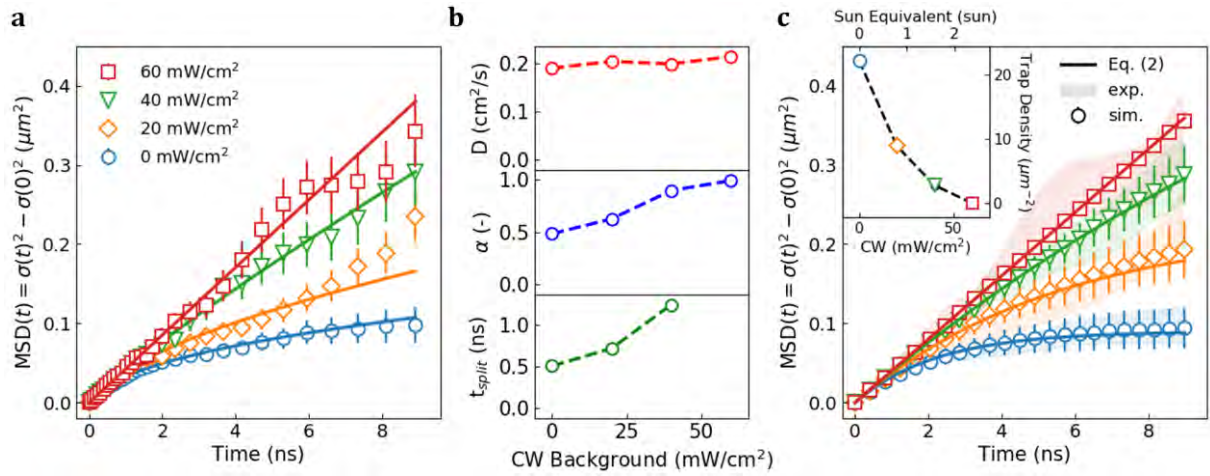


Figure 2. (a) Mean-square-displacement of the exciton population for different continuous wave (CW) background intensities. Experimental values are displayed with open markers, while the fit functions (equation S3), defined through the parameters D , α , and t_{split} , are displayed as solid lines. (b) Diffusivity D , diffusion exponent α , and the onset of subdiffusive regime t_{split} extracted from fits in a). (c) Theoretical model (equation (2), solid lines), and numerical simulation (open markers) for exciton diffusion with different trap densities. Experimental values from a) are displayed as shaded areas for comparison. The inset shows the trap densities found with the simulations. Mirror axis of the inset is the sun equivalent of the background illumination intensity (AM1.5 Global and $E_{\text{photon}} > E_{\text{bandgap}}$).

Importantly, the early diffusion dynamics are unaffected by the trap density. This gives us direct access to the intrinsic exciton diffusivity of the material and allows us to compare the exciton diffusivity between perovskites of different composition. To explore compositional variations, we substitute phenethylammonium (PEA) with butylammonium (BA) - another commonly used spacer molecule for two-dimensional perovskites.^{20,28,29,32,43,52–54}

Figure 3a displays the MSD of the (BA)₂PbI₄ perovskite, again showing the distinct transition from normal diffusion to a subdiffusive regime. However, as compared to (PEA)₂PbI₄, excitons in (BA)₂PbI₄ are remarkably less mobile, displaying a diffusivity of only $0.013 \pm 0.002 \text{ cm}^2/\text{s}$, which is over an order of magnitude smaller than that of (PEA)₂PbI₄ with $0.192 \pm 0.013 \text{ cm}^2/\text{s}$ (green curve shown in Figure 3a for comparison). Taking the exciton lifetime into account, the difference in diffusivity results in a reduction in the diffusion length from $236 \pm 4 \text{ nm}$ for (PEA)₂PbI₄ to a mere $39 \pm 8 \text{ nm}$ for (BA)₂PbI₄ (see Figure 3b). These results indicate that the choice of ligand plays a crucial role in controlling the spatial dynamics of excitons in two-dimensional perovskites. We would like to note that the reported diffusion lengths follow the literature convention of diffusion lengths in one dimension, as it is the relevant length scale for device design. The actual two-dimensional diffusion length is greater by a factor of $\sqrt{2}$.

To understand the large difference in diffusivity between (PEA)₂PbI₄ and (BA)₂PbI₄, we take a closer look at the structural differences between these two materials. Changing the organic spacer can have a significant influence on the structural and optoelectronic properties of 2D perovskites. Specifically, increasing the cross-sectional area of the organic spacer distorts the inorganic lattice and reduces the orbital overlap between neighboring octahedra, which in turn increases the effective mass of the exciton.⁵⁵ Comparing the octahedral tilt angles of (PEA)₂PbI₄ and (BA)₂PbI₄, a larger distortion for the bulkier (PEA)₂PbI₄ (152.8°) as compared to (BA)₂PbI₄ (155.1°) is found.^{56,57} The *larger* exciton effective mass in (PEA)₂PbI₄ would, however, suggest *slower* diffusion, meaning a simple effective mass picture for free excitons cannot explain the observed trend in the diffusivity between (PEA)₂PbI₄ and (BA)₂PbI₄.

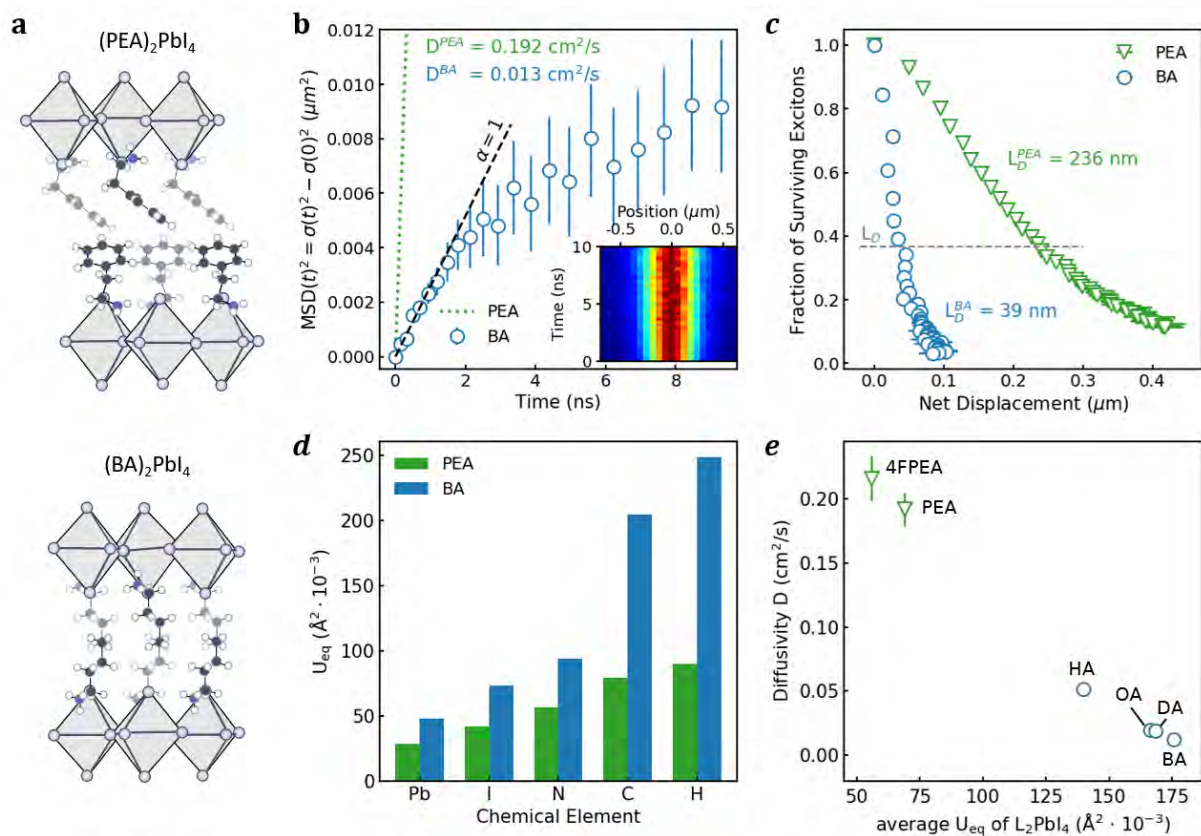


Figure 3. (a) $(\text{PEA})_2\text{PbI}_4$ and $(\text{BA})_2\text{PbI}_4$ crystal structure.^{56,57} (b) Mean-square-displacement of exciton population over time for $(\text{PEA})_2\text{PbI}_4$ (dotted line) and $(\text{BA})_2\text{PbI}_4$ (circles). Inset shows the normalized fluorescence emission intensity $I(x,t)$ for $(\text{BA})_2\text{PbI}_4$. (c) Fractions of surviving excitons (extracted from lifetime data in Figure S7) vs. net spatial displacement $\sqrt{\text{MSD}(t)}$ of excitons for $(\text{PEA})_2\text{PbI}_4$ (triangles) and $(\text{BA})_2\text{PbI}_4$ (circles). (d) Average atomic displacement U_{eq} of the chemical elements in $(\text{PEA})_2\text{PbI}_4$ and $(\text{BA})_2\text{PbI}_4$. Data was extracted from previously published single crystal x-ray diffraction data.^{56,57} (e) Diffusivity D vs. average atomic displacement U_{eq} for different organic spacers: 4-fluoro-phenethylammonium (4FPEA),⁵⁸ phenethylammonium (PEA),⁵⁶ hexylammonium (HA),⁵⁷ octylammonium (OA),⁵⁹ decylammonium (DA),⁵⁹ Butylammonium (HA).⁵⁷

Rather than dealing with free excitons, a number of studies have pointed at the importance of strong exciton-phonon coupling and the formation of exciton-polarons in perovskite materials.^{35,37,60,61} In the presence of an exciton, the soft inorganic lattice of the perovskite can be easily distorted through coupling with phonons, leading to the formation of polarons. As compared to a free exciton, an exciton-polaron exhibits a larger effective mass and, consequently, a lower diffusivity. The softer the lattice, the larger the distortion, and the heavier the polaron effective mass will be.⁶² The correct theoretical description of the polaron in 2D perovskites is the subject of ongoing debate, though the current consensus is that the polar anharmonic lattice requires a description beyond conventional Frohlich theory.^{60,61,63}

To investigate the potential role of polaron formation on exciton diffusion, we first quantify the softness of the lattices of both (PEA)₂PbI₄ and (BA)₂PbI₄ by extracting the atomic displacement parameters from their respective single crystal x-ray data.⁶⁴ The atomic displacement of the different atoms of both systems are summarized in Figure 3d, showing distinctly larger displacements for (BA)₂PbI₄ as compared to (PEA)₂PbI₄ in both the organic and inorganic sublattice.^{56,57} The increased lattice rigidity for (PEA)₂PbI₄ can be attributed to the formation of an extensive network of pi-hydrogen bonds and a more space-filling nature of the aromatic ring, both of which are absent in the aliphatic BA spacer molecule. Qualitatively, a stiffening of the lattice reduces the exciton-phonon coupling and would explain the observed higher diffusivity in (PEA)₂PbI₄ as compared to (BA)₂PbI₄. In addition to a softer lattice, we find that (BA)₂PbI₄ exhibits a larger exciton-phonon coupling strength as compared to (PEA)₂PbI₄, as confirmed by analyzing the temperature-dependent broadening of the photoluminescence linewidth of the two materials (see also Figure S8-S10 and Table S2).⁶⁵ The combined effect of a softer lattice and a larger exciton-phonon coupling strength in (BA)₂PbI₄ as compared to (PEA)₂PbI₄ promotes the formation of exciton-polarons with heavier effective masses, consistent with the observed trend in the diffusivity.

To further test the correlation between lattice softness and diffusivity, we have performed measurements on a wider range of two-dimensional perovskites with different organic spacers. In

Figure 3e, we present the diffusivity as a function of average atomic displacement for each of the different perovskite unit cells. Across the entire range of organic spacers, a clear correlation between the diffusivity and the lattice softness is found, consistent with exciton-polaron formation as the dominant parameter in determining the spatial dynamics of the excited state.

Finally, we look at the temperature dependence of the diffusivity, which can give us critical insights into the nature of the polaron. When long-range deformations of the lattice are dominant, the exciton-polaron extends across multiple lattice sites and is categorized as a large polaron. The diffusion of large polarons occurs coherently and decreases with increasing temperature ($\partial D/\partial T < 0$), resembling that of band-like free exciton motion, although with a strongly increased effective mass. Contrarily, in the case of dominant short-range lattice deformations, small polarons are formed that localize within the unit cell of the material. The motion of small polarons occurs through incoherent site-to-site hopping and increases with temperature ($\partial D/\partial T > 0$). In both $(\text{PEA})_2\text{PbI}_4$ and $(\text{BA})_2\text{PbI}_4$, a clear negative scaling of the diffusivity with temperature is observed ($\partial D/\partial T < 0$, see Figure 4), consistent with the formation of large exciton-polarons and coherent exciton transport through the 2D plane.

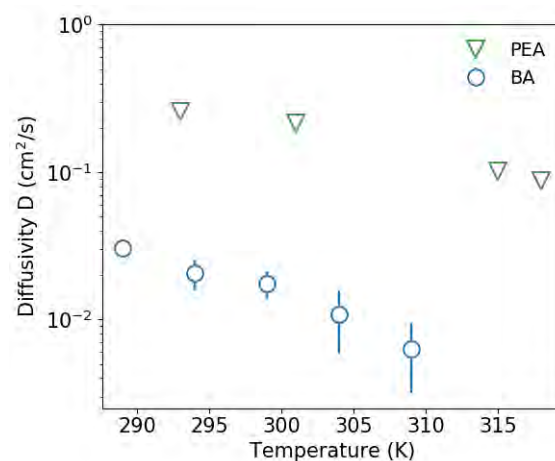


Figure 4. Temperature dependent diffusivity in $(\text{PEA})_2\text{PbI}_4$ (triangles) and $(\text{BA})_2\text{PbI}_4$ (circles).

Discussion

Given the apparent importance of exciton-phonon coupling in the spatial dynamics of excitons in 2D perovskites, structural rigidity becomes a critical design parameter in these systems. Taking into account the close correlation between diffusivity and the atomic displacement, this parameter space can be readily explored using available x-ray crystal structure data for many 2D perovskite analogues. While the influence of the organic spacer is expected to be particularly strong in the class of $n = 1$ 2D perovskites, we have observed consistent trends in the $n = 2$ analogues. Indeed, just like in $n = 1$, in $n = 2$ the use of the PEA cation yields higher diffusivities than for BA (see supporting information). Similarly, the interstitial formamidinium (FA) cation in $n = 2$ yields higher diffusivity than the methylammonium (MA) cation, consistent with the trend in the atomic displacement parameters.

From a technological perspective, structural rigidity may play a particularly important role in light emitting devices. Long exciton diffusion lengths in light emitting applications can act detrimentally on device performance, as it increases the possibility of encountering a trapping site. From an exciton-polaron perspective, this suggests soft lattices are preferred. At the same time though, Gong et al. highlighted the role of structural rigidity in improving the luminescence quantum yield through a reduced coupling to non-radiative decay pathways.^{64,66} A trade-off therefore exists in choosing the optimal rigidity for bright emission. Meanwhile, for light harvesting applications, long diffusion lengths are essential for the successful extraction of excitons. While strongly excitonic 2D perovskites are generally to be avoided due to the penalty imposed by the exciton binding energy, improving the understanding of the spatial dynamics of the excitonic state may help mitigate this negative impact of the thinnest members of the 2D perovskites in solar harvesting.

Acknowledgements

This work has been supported by the Spanish Ministry of Economy and Competitiveness through The “María de Maeztu” Program for Units of Excellence in R&D (MDM-2014-0377). M.S. acknowledges the financial support of a fellowship from “la Caixa” Foundation (ID 100010434). The fellowship code is LCF/BQ/IN17/11620040. M.S. has received funding from the European Union’s Horizon 2020 research and innovation program under the Marie Skłodowska-Curie grant agreement No. 713673. F.P. acknowledges support from the Spanish Ministry for Science, Innovation, and Universities through the state program (PGC2018-097236-A-I00) and through the Ramón y Cajal program (RYC-2017-23253), as well as the Comunidad de Madrid Talent Program for Experienced Researchers (2016-T1/IND-1209). N.A., M.M. and R.D.B. acknowledges support from the Spanish Ministry of Economy, Industry and Competitiveness through Grant FIS2017-86007-C3-1-P (AEI/FEDER, EU). E.P. acknowledges support from the Spanish Ministry of Economy, Industry and Competitiveness through Grant FIS2016-80434-P (AEI/FEDER, EU), the Ramón y Cajal program (RYC-2011- 09345) and the Comunidad de Madrid through Grant S2018/NMT-4511 (NMAT2D-CM). S.P. acknowledges financial support by the VILLUM FONDEN via the Centre of Excellence for Dirac Materials (Grant No. 11744).

Author contributions

M.S. and F.P. designed this study. M.S. led the experimental work and processing of experimental data. M.S. set up the diffusion measurement technique with the assistance of T.J.L., and S.W.W. A.J.M. and M.S. performed temperature dependent measurements. M.S. and A.J.M. prepared perovskite materials. N.A., M.M., and R.D.B. performed theoretical and numerical modelling of exciton transport. M.S, F.P., S.P., and E.P. provided the theoretical interpretation of the intrinsic exciton transport. F.P. supervised the project. M.S. and F.P. wrote the original draft of the manuscript. All authors contributed to reviewing the manuscript.

References

1. Kojima, A., Miyasaka, T., Teshima, K. & Shirai, Y. Organometal halide perovskites as visible-light sensitizers for photovoltaic cells. *J. Am. Chem. Soc.* **131**, 6050–6051 (2009).
2. Burschka, J. *et al.* Sequential deposition as a route to high-performance perovskite-sensitized solar cells. *Nature* **499**, 316–319 (2013).
3. Liu, M., Johnston, M. B. & Snaith, H. J. Efficient planar heterojunction perovskite solar cells by vapour deposition. *Nature* **501**, 395–398 (2013).
4. Yang, W. S. *et al.* High-performance photovoltaic perovskite layers fabricated through intramolecular exchange. *Science* **348**, 1234–1237 (2015).
5. Green, M. A., Ho-Baillie, A. & Snaith, H. J. The emergence of perovskite solar cells. *Nat. Photonics* **8**, 506–514 (2014).
6. Veldhuis, S. A. *et al.* Perovskite Materials for Light-Emitting Diodes and Lasers. *Adv. Mater.* **28**, 6804–6834 (2016).
7. Tan, Z.-K. *et al.* Bright light-emitting diodes based on organometal halide perovskite. *Nat. Nanotechnol.* **9**, 687–692 (2014).
8. Stranks, S. D. *et al.* Electron-hole diffusion lengths exceeding 1 micrometer in an organometal trihalide perovskite absorber. *Science* **342**, 341–344 (2013).
9. Shi, D. *et al.* Low trap-state density and long carrier diffusion in organolead trihalide perovskite single crystals. *Science* **347**, 519–522 (2015).
10. Yin, W. J., Shi, T. & Yan, Y. Unusual defect physics in CH₃NH₃PbI₃ perovskite solar cell absorber. *Appl. Phys. Lett.* **104**, (2014).
11. Brandt, R. E., Stevanović, V., Ginley, D. S. & Buonassisi, T. Identifying defect-tolerant semiconductors with high minority-carrier lifetimes: Beyond hybrid lead halide perovskites.

- MRS Commun.* **5**, 265–275 (2015).
12. Steirer, K. X. *et al.* Defect Tolerance in Methylammonium Lead Triiodide Perovskite. *ACS Energy Lett.* **1**, 360–366 (2016).
 13. Protesescu, L. *et al.* Nanocrystals of Cesium Lead Halide Perovskites (CsPbX₃, X = Cl, Br, and I): Novel Optoelectronic Materials Showing Bright Emission with Wide Color Gamut. *Nano Lett.* **15**, 3692–3696 (2015).
 14. Weidman, M. C., Seitz, M., Stranks, S. D. & Tisdale, W. A. Highly Tunable Colloidal Perovskite Nanoplatelets through Variable Cation, Metal, and Halide Composition. *ACS Nano* **10**, 7830–7839 (2016).
 15. Shamsi, J., Urban, A. S., Imran, M., De Trizio, L. & Manna, L. Metal Halide Perovskite Nanocrystals: Synthesis, Post-Synthesis Modifications, and Their Optical Properties. *Chem. Rev.* (2019).
 16. Jena, A. K., Kulkarni, A. & Miyasaka, T. Halide Perovskite Photovoltaics: Background, Status, and Future Prospects. *Chem. Rev.* **119**, 3036–3103 (2019).
 17. Niu, G., Guo, X. & Wang, L. Review of recent progress in chemical stability of perovskite solar cells. *J. Mater. Chem. A* **3**, 8970–8980 (2015).
 18. Berhe, T. A. *et al.* Organometal halide perovskite solar cells: Degradation and stability. *Energy Environ. Sci.* **9**, 323–356 (2016).
 19. Yang, S., Fu, W., Zhang, Z., Chen, H. & Li, C. Z. Recent advances in perovskite solar cells: Efficiency, stability and lead-free perovskite. *J. Mater. Chem. A* **5**, 11462–11482 (2017).
 20. Smith, I. C., Hoke, E. T., Solis-Ibarra, D., McGehee, M. D. & Karunadasa, H. I. A Layered Hybrid Perovskite Solar-Cell Absorber with Enhanced Moisture Stability. *Angew. Chemie Int. Ed.* **53**, 11232–11235 (2014).

21. Fu, Q. *et al.* Recent Progress on the Long-Term Stability of Perovskite Solar Cells. *Adv. Sci.* **5**, (2018).
22. Quan, L. N. *et al.* Ligand-Stabilized Reduced-Dimensionality Perovskites. *J. Am. Chem. Soc.* **138**, 2649–2655 (2016).
23. Yang, S., Fu, W., Zhang, Z., Chen, H. & Li, C. Z. Recent advances in perovskite solar cells: Efficiency, stability and lead-free perovskite. *J. Mat. Chem. A.* **5**, 11462–11482 (2017).
24. Liu, Y. *et al.* Ultrahydrophobic 3D/2D fluoroarene bilayer-based water-resistant perovskite solar cells with efficiencies exceeding 22%. *Sci. Adv.* **5**, (2019).
25. Grancini, G. *et al.* One-Year stable perovskite solar cells by 2D/3D interface engineering. *Nat. Commun.* **8**, 1–8 (2017).
26. Yang, R. *et al.* Oriented Quasi-2D Perovskites for High Performance Optoelectronic Devices. *Adv. Mater.* **30**, 1804771 (2018).
27. Ortiz-Cervantes, C., Carmona-Monroy, P. & Solis-Ibarra, D. Two-Dimensional Halide Perovskites in Solar Cells: 2D or not 2D? *ChemSusChem* **12**, 1560–1575 (2019).
28. Tsai, H. *et al.* Stable Light-Emitting Diodes Using Phase-Pure Ruddlesden-Popper Layered Perovskites. *Adv. Mater.* **30**, 1704217 (2018).
29. Xing, J. *et al.* Color-stable highly luminescent sky-blue perovskite light-emitting diodes. *Nat. Commun.* **9**, (2018).
30. Lin, Y. *et al.* Suppressed Ion Migration in Low-Dimensional Perovskites. *ACS Energy Lett.* **2**, 1571–1572 (2017).
31. Zhang, L., Liu, Y., Yang, Z. & Liu, S. (Frank). Two dimensional metal halide perovskites: Promising candidates for light-emitting diodes. *Journal of Energy Chemistry* **37**, 97–110 (2019).
32. Yuan, M. *et al.* Perovskite energy funnels for efficient light-emitting diodes. *Nat. Nanotechnol.*

- 11**, 872–877 (2016).
33. Kumar, S. *et al.* Efficient Blue Electroluminescence Using Quantum-Confined Two-Dimensional Perovskites. *ACS Nano* **10**, 9720–9729 (2016).
 34. Congreve, D. N. *et al.* Tunable Light-Emitting Diodes Utilizing Quantum-Confined Layered Perovskite Emitters. *ACS Photonics* **4**, 476–481 (2017).
 35. Straus, D. B. & Kagan, C. R. Electrons, Excitons, and Phonons in Two-Dimensional Hybrid Perovskites: Connecting Structural, Optical, and Electronic Properties. *J. Phys. Chem. Lett.* **9**, 1434–1447 (2018).
 36. Mao, L., Stoumpos, C. C. & Kanatzidis, M. G. Two-Dimensional Hybrid Halide Perovskites: Principles and Promises. *J. Am. Chem. Soc.* **141**, 1171–1190 (2019).
 37. Mauck, C. M. & Tisdale, W. A. Excitons in 2D Organic–Inorganic Halide Perovskites. *Trends in Chemistry* **1**, 380–393 (2019).
 38. Katan, C., Mercier, N. & Even, J. Quantum and Dielectric Confinement Effects in Lower-Dimensional Hybrid Perovskite Semiconductors. *Chem. Rev.* **119**, 3140–3192 (2019).
 39. D’Innocenzo, V. *et al.* Excitons versus free charges in organo-lead tri-halide perovskites. *Nat. Commun.* **5**, (2014).
 40. Blancon, J. C. *et al.* Scaling law for excitons in 2D perovskite quantum wells. *Nat. Commun.* **9**, (2018).
 41. Papavassiliou, G. C. Three- and Low-Dimensional Inorganic Semiconductors. *Progress in Solid State Chemistry* **25**, 125–270 (1997).
 42. Chong, W. K., Giovanni, D. & Sum, T.-C. Excitonics in 2D Perovskites. in *Halide Perovskites* 55–79 (Wiley, 2018).
 43. Ortiz-Cervantes, C., Carmona-Monroy, P. & Solis-Ibarra, D. Two-Dimensional Halide Perovskites

- in Solar Cells: 2D or not 2D? *ChemSusChem* **12**, 1560–1575 (2019).
44. Luque, A. & Hegedus, S. *Handbook of Photovoltaic Science and Engineering*. (John Wiley & Sons, Ltd, 2003).
 45. Blancon, J. C. *et al.* Extremely efficient internal exciton dissociation through edge states in layered 2D perovskites. *Science* **355**, 1288–1292 (2017).
 46. Akselrod, G. M. *et al.* Visualization of exciton transport in ordered and disordered molecular solids. *Nat. Commun.* **5**, (2014).
 47. Seitz, M., Gant, P., Castellanos-Gomez, A. & Prins, F. Long-Term Stabilization of Two-Dimensional Perovskites by Encapsulation with Hexagonal Boron Nitride. *Nanomaterials* **9**, 1120 (2019).
 48. Yaffe, O. *et al.* Excitons in ultrathin organic-inorganic perovskite crystals. *Phys. Rev. B* **92**, 045414 (2015).
 49. Ha, S. T., Shen, C., Zhang, J. & Xiong, Q. Laser cooling of organic-inorganic lead halide perovskites. *Nat. Photonics* **10**, 115–121 (2016).
 50. Akselrod, G. M. *et al.* Subdiffusive Exciton Transport in Quantum Dot Solids. *Nano Lett.* **14**, 3556–3562 (2014).
 51. Wu, X. *et al.* Trap States in Lead Iodide Perovskites. *J. Am. Chem. Soc.* **137**, 2089–2096 (2015).
 52. Fu, W. *et al.* Two-Dimensional Perovskite Solar Cells with 14.1% Power Conversion Efficiency and 0.68% External Radiative Efficiency. *ACS Energy Lett.* **3**, 2086–2093 (2018).
 53. Cao, D. H., Stoumpos, C. C., Farha, O. K., Hupp, J. T. & Kanatzidis, M. G. 2D Homologous Perovskites as Light-Absorbing Materials for Solar Cell Applications. *J. Am. Chem. Soc.* **137**, 7843–7850 (2015).
 54. Lian, X. *et al.* Two-dimensional inverted planar perovskite solar cells with efficiency over 15%:

- Via solvent and interface engineering. *J. Mater. Chem. A* **7**, 18980–18986 (2019).
55. Lee, J. H. *et al.* Resolving the Physical Origin of Octahedral Tilting in Halide Perovskites. *Chem. Mater.* **28**, 4259–4266 (2016).
 56. Du, K. Z. *et al.* Two-Dimensional Lead(II) Halide-Based Hybrid Perovskites Templated by Acene Alkylamines: Crystal Structures, Optical Properties, and Piezoelectricity. *Inorg. Chem.* **56**, 9291–9302 (2017).
 57. Billing, D. G. & Lemmerer, A. Synthesis, characterization and phase transitions in the inorganic–organic layered perovskite-type research papers. *Acta Crystallogr. Sect. B* **63**, 735–747 (2007).
 58. Hu, J. *et al.* Synthetic control over orientational degeneracy of spacer cations enhances solar cell efficiency in two-dimensional perovskites. *Nat. Commun.* **10**, (2019).
 59. Lemmerer, A. & Billing, D. G. Synthesis, characterization and phase transitions of the inorganic-organic layered perovskite-type hybrids $[(C_nH_{2n+1}NH_3)_2PbI_4]$, $n = 7, 8, 9$ and 10 . *Dalt. Trans.* **41**, 1146–1157 (2012).
 60. Zhu, H. *et al.* Screening in crystalline liquids protects energetic carriers in hybrid perovskites. *Science* **353**, 1409–1413 (2016).
 61. Katan, C., Mohite, A. D. & Even, J. Entropy in halide perovskites. *Nat. Mater.* **17**, 277–279 (2018).
 62. Emin, D. *Polarons*. *Polarons* (Cambridge University Press, 2010).
 63. Guo, Y. *et al.* Dynamic emission Stokes shift and liquid-like dielectric solvation of band edge carriers in lead-halide perovskites. *Nat. Commun.* **10**, (2019).
 64. Gong, X. *et al.* Electron-phonon interaction in efficient perovskite blue emitters. *Nat. Mater.* **17**, 550–556 (2018).
 65. Rudin, S., Reinecke, T. L. & Segall, B. *Temperature-dependent exciton linewidths in semiconductors*. *Phys. Rev. B* **42**, (1990).

66. He, J., Fang, W. H., Long, R. & Prezhdo, O. V. Increased Lattice Stiffness Suppresses Nonradiative Charge Recombination in MAPbI₃ Doped with Larger Cations: Time-Domain Ab Initio Analysis. *ACS Energy Lett.* **3**, 2070–2076 (2018).